II International Conference on Simulation for Additive Manufacturing - Sim-AM 2019
F. Auricchio, E. Rank, P. Steinmann, S. Kollmannsberger and S. Morganti (Eds)

PARAMETRIC STUDY IN CO-EXTRUSION-BASED ADDITIVE MANUFACTURING OF CONTINUOUS FIBER-REINFORCED PLASTIC COMPOSITES

Sim-AM 2019

HANNY ALBRECHT[1], CHETHAN SAVANDAIAH[*,2], ALEXANDER LEPSCHI[2], BERNHARD LÖW-BASELLI[1], AND ANDREAS HAIDER[2]

[1]Institute of Polymer Extrusion and Compounding
Johannes Kepler University
Altenberger Strasse 69, 4040 Linz, Austria
e-mail: hanny.albrecht@jku.at, web page: https://www.jku.at/ipec

[*], [2]Kompetenzzentrum Holz GmbH
Altenberger Strasse 69, 4040 Linz, Austria
e-mail: c.savandaiah@wood-kplus.at, web page: https://www.wood-kplus.at

*Corresponding author

Keywords: Additive manufacturing, Continuous carbon fiber, Numerical simulation, Composite co-extrusion

Abstract

The main objective of this research is to investigate the newly designed geometry and process parameters in a dual matrix composite filament co-extrusion technology (CFC), a co-extrusion of continuous carbon fiber pre-impregnated with thermoset (1.5K) also known as composite carbon fiber (CCF) filament with a special binder thermoplastic filament.
Accordingly, non-isothermal fluid flow and particle tracking analysis were employed in order to examine the melt flow dynamics. In addition, critical parameters like pressure drop, velocity, shear stress, residence time, and swelling/shrinkage ratio were evaluated.
In particular, the computational fluid dynamics (CFD) simulations indicates distress in the conventional die design, recirculation and stagnation of melt flow in the dead zones causing longer melt residence leading to the thermal degradation of thermoplastic material.
Furthermore, a new print head was designed to expedite the solution for the possible flow instabilities that may lead to a disparity in the material and mechanical properties, a side- fed mandrel die was used as a melt distributor. Consequently, the side- fed mandrel die ensured a homogeneous melt distribution inside the CFC print head, particularly at the die exit.

1 INTRODUCTION

The advancement in Additive manufacturing (AM) has catered the need of the lightweight design industries like automotive and aerospace, where a high strength to weight ratio is a crucial aspect, as an alternative manufacturing method to produce high-performance composite materials [1]. Specifically, in the field of fused filament fabrication (FFF), the

different processing methods have evolved into the industrial-grade application such as big area additive manufacturing, composite FFF and the newly developed CFC.
The advanced CFC method involves the inclusion of endless carbon fiber reinforcement into the molten thermoplastic polymer; the synergy of high strength to weight ratio of endless carbon fiber and the ease of processing of thermoplastic is accomplished, which is an essential property of high-performance lightweight materials. Furthermore, with design optimization, the properties of the final printed part can be improved, whereby the modulus and strength of the material may be improved up to 4 to 6 times [1]. Moreover, in order to elevate the need for high strength to weight ratio and defect free printed composite part, a new print head design based on the 1st generation CFC print head is being considered. This is achieved by identifying the critical issues associated with the current design and addressing them in newly designed side- fed mandrel print head. Furthermore, the side-fed mandrel die is being used in the extrusion industry for decades as a melt distributor is also beneficial for the CFC print head, the die can distribute the polymer melt uniformly through the melting chamber and eliminate recirculation flow problem observed in the 1st generation CFC.
Furthermore, Bellini et al., Ramanath et al., and Turner et al., [2-4] had discussed about several models used for calculating pressure and temperature distribution of neat filament without fiber inclusion in the conventional print head.
In the present work, authors performed CFD simulation on both, 1st generation and the newly designed CFC print head, and investigated the critical parameters such as pressure drop, velocity shear stress, residence time, and swelling/shrinkage ratio, to mitigate the understanding of the CFC printing process.

2 PRINTING PROCESS

A straight extrusion flow model combined with heat transfer is assumed due to the first-stage process of the CFC resembles conventional extrusion-based additive manufacturing. Furthermore, the melt flow process with CCF filament is analogous to coating process in a pressure-type die. The 1st generation CFC and modified CFC print head are illustrated in figure 1 (a) and (b), respectively.

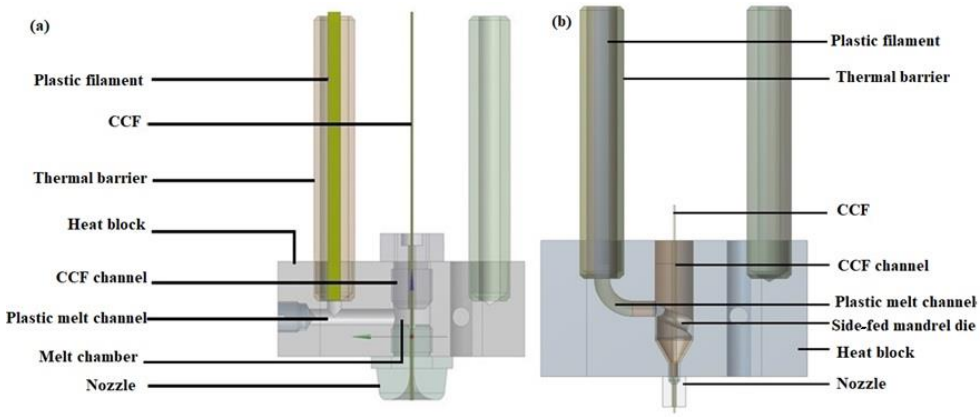

Figure 1: Schematics of the print heads, (a) 1st generation CFC print head, (b) Modified CFC print head with side- fed mandrel die

In Figure 1 (a) and Figure 1 (b), a thermoplastic filament with 1.75 mm diameter is fed through the lateral channel covered by a thermal barrier, which restricts the high gradient thermal variation in the plastic filament to ensure the solid state before entering the melting channel. In the melting channel, the filament is being heated into a semi-viscous state. Meanwhile, CCF filament is being fed through the CCF channel and goes through the inner bore of the fiber inlet. Herein, as the CCF enters the inner zone of the melt chamber it is coated with the molten thermoplastic polymer and subsequently, the dual matrix composite is extruded through nozzle outlet and is deposited on a print bed.

3 MATERIAL AND METHODOLOGY

3.1 Material

In this study, the most common printing material Polylactide (PLA) polymer was used, PLA grade REVODE190 was purchased from Zhejiang Hisun Biomaterials Co., Ltd. The rheological characterization of the PLA was performed in Anton Paar MCR-502; a plate-plate methodology was used to determine the viscosity, storage- and loss modulus. The experiments were performed at two temperatures, 190 °C and 210 °C. The measurement data with its fitting are plotted in Figure 2 (a) and Figure 2 (b), and the model parameters are listed in Table 1 and Table 2. The CCF is a 1.5k grade carbon-fiber tow pre-impregnated with a thermoset resin, has an effective diameter of 0.37 mm.

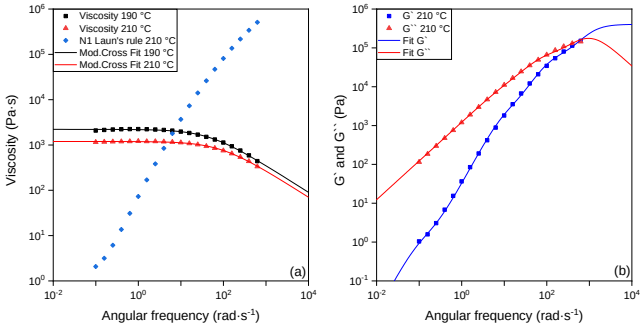

Figure 2: (a) Shear viscosity of PLA at 190 °C and 210 °C fitted with the modified Cross model, first normal stress difference N1 is calculated with Laun's rule [5]; (b) Experimental G' and G" of PLA sample obtained at 210°C.

Table 1: Kaye – Bernstein Kearsley Zapas (K-BKZ) model parameters for PLA at T = 210°C (α = 8.78, β = 0.74, θ = 0, $\bar{\lambda}$ = 1.94 s) and Arrhenius approximation law parameter (α = 0.03, T_0 = 483.15)

k	λ_k	a_k
	[s]	[Pa]
1	0.001	3.44E+05
2	0.01	6.07E+04
3	0.1	2.27E+03
4	1	1.15E+01
5	10	1.12E-04
6	100	2.31E-01

Table 2: Modified Cross model parameters for PLA at T = 210°C and other material constants

Parameter	Unit	Value
η_0	Pa.s	1194.31
λ	s	0.011
m	-	0.597
α	K^{-1}	0.031
T_0	K	483.15
ρ_m	kg/m^3	1096.51
κ	W/m K	0.13
C_p	J/(kg K)	2237

3.2 Governing equations

Steady, creeping, incompressible non-isothermal flow of polymer melts inside the heat block is considered for the purpose of computational fluid dynamic simulations. In this study, two different constitutive equations for defining the extra stress tensor τ are proposed. The inelastic viscous stress component τ_s, in which the shear-rate dependence viscosity is represented by a modified Cross model:

$$\eta(\dot{\gamma}) = \frac{\eta_0}{(1+\lambda\dot{\gamma})^m} \tag{1}$$

Where η_o is the zero shear viscosity (Pa.s), λ is a natural time (s), $\dot{\gamma}$ is the shear rate which is a second invariant of the rate deformation tensor (s^{-1}), m is the Cross-law index. In addition, the (K-BKZ) [6] is applied for the viscoelastic extra-stress τ_p and the given equation as follows:

$$\tau_p = \frac{1}{1-\theta}\int_{-\infty}^{t}\sum_{k=1}^{N}\frac{a_k}{\lambda_k}\exp\left(-\frac{t-t'}{\lambda_k}\right)\left(\frac{\alpha}{(\alpha-3)+\beta I_{C^{-1}}+(1-\beta)I_C}\right)\left[C_t^{-1}(t')+\theta C_t(t')\right]dt' \tag{2}$$

where a_k and λ_k are the relaxation modulus and relaxation time for mode k, t is the current time, N is the number of relaxation modes, α and β are non-linear material constants, θ is a scalar parameter that controls the ratio of the normal stress differences, I_c and I_c^{-1} are the first invariants of the Cauchy-Green strain tensor C_t and its inverse C_t^{-1}, the Finger strain tensor.
The temperature shift factor examined in this study is given by the approximate Arrhenius law:

$$a_T = \exp\left(-\alpha\left(T-T_0\right)\right) \tag{3}$$

Where α is the material coefficient (K^{-1}), T_0 is the reference temperature (K). The shear thinning behavior and melt temperature observed in thermoplastic material used in 3D-printing has a direct influence on the pressure drop across the system [3]. Furthermore, the melt temperature is one of the critical parameters for the process, since it increases due to

viscous dissipation caused by the shearing effect at the nozzle [4]. The viscosity of the melt changes not only with the shear rate but also with temperature, which leads to the alteration of the shape of the dual matrix extrudate. Moreover, to impede the material degradation due to high temperature rise and cause decline in mechanical properties, herein, numerical simulation is being applied to optimize the CFC processing conditions.

4 CFD SIMULATION

Numerical simulations were carried out using ANSYS Polyflow and Fluent software. A three-dimensional generalized Newtonian fluid flow analysis was conducted, firstly, the entire extruder geometry was considered, and then only on nozzle domain. A simplification was applied in nozzle geometry; an axisymmetric two-dimensional analysis was performed. Moreover, all analyses are a coupled problem of melt flow and heat transfer.

4.1 Boundary conditions and processing parameters

During the extrusion of the thermoplastic filament, plug flow is assumed at the entrance of the melting chamber due to the solid state of the filament at that region. In order to avoid clogging of the material, it should be taken into consideration that the plastic filament has a slower feed rate than the reinforcing fiber. In this analysis, plastic feed rate varies between 6 – 8% of reinforcing fiber feed that varies from 60 mm/min up to 1500 mm/min. The entry temperature at the melting chamber is calculated from steady thermal analysis, where only the energy equation is being solved. As for the two-dimensional nozzle model, a fully developed velocity profile corresponding to a given flow rate along the inflow boundary and a uniform polymer temperature as in the nozzle wall is being imposed. Since the reinforced composite fiber is continuous and rather stiff, hence it is assumed that it acts like a moving solid, where the tangential velocity is imposed with the value of fiber feed rate. Non-slip boundary condition with all velocity components being set to zero and fixed temperature are imposed along the wall. At the nozzle exit region a constant pressure outlet boundary conditions are applied. The air temperature at the entrance and exit was assumed to be the same as ambient temperature, 297.15 K. As for the extrudate swell analysis, the computational domain is extended with a free surface region, which has zero stresses and convective cooling boundary condition.

5 RESULTS AND DISCUSSIONS

5.1 Effect of design geometry

Prior to the CFD simulation with modified CFC print head, simulation in 1st generation CFC print head was performed in order to evaluate the flow pattern, pressure drop and melt residence time inside the print head. In Figure 3, the flow of polymer melt through the melt chamber in both, 1st generation CFC print head and modified side- fed CFC print head are illustrated. Evidently, in Figure 3 (a) some stagnation and recirculation of the melt flow in the 1st generation CFC print head were observed, which may result in longer residence time causing material disparities. Moreover, strong recirculation flow forming a secondary vortex was found in the left zone from the primary flow direction. In addition, another recirculation flow region was observed as the melt encountered the drag flow of composite fiber.

Furthermore, several simulations were performed for varied fiber feed rates, U = 60 mm/min (Low), 900 mm/min (Moderate), and 1500 mm/min (High) in order to investigate the melt flow behavior in the modified CFC print head. As for the plastic filament feed rate, the set-up with 7% of fiber feed rate was chosen based on the extrudate swell calculation, see section 5.2. In Figure 3 (b), Figure 3(c) and Figure 3(d) show the streamlines of velocity magnitude in the flow domain. The modified CFC print head delivers a flow enhancement, thus the polymer melt conveys smoothly from the melting chamber entrance to the nozzle exit without any appearance of stagnation and recirculation flow. Furthermore, Figure 4 illustrates that the largest gradient of pressure- drop occurred especially in the nozzle part. With the utilization of the new design, a significant reduction of pressure drop is achieved, so that better print resolution can be obtained.

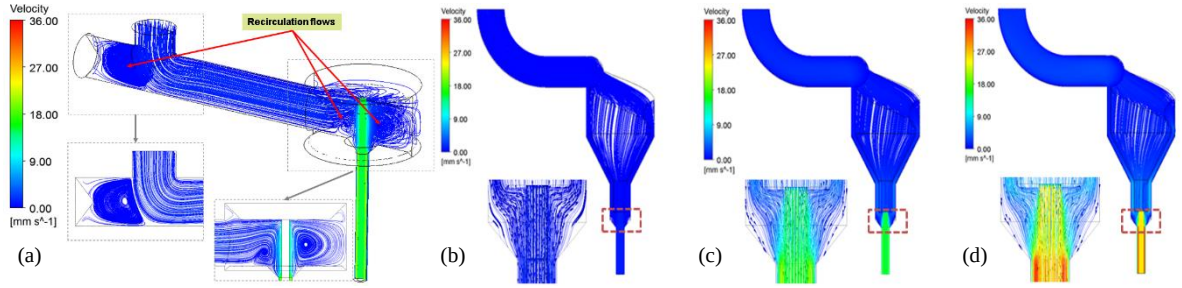

Figure 3: Streamlines of the 1st generation CFC print head and modified side- fed CFC print head; 1st generation, (a) U = 900 mm/min; modified side- fed CFC print head, (b) L/D=5, U = 60 mm/min (c) L/D=5, U = 900 mm/min (d) L/D=5, U = 1500 mm/min

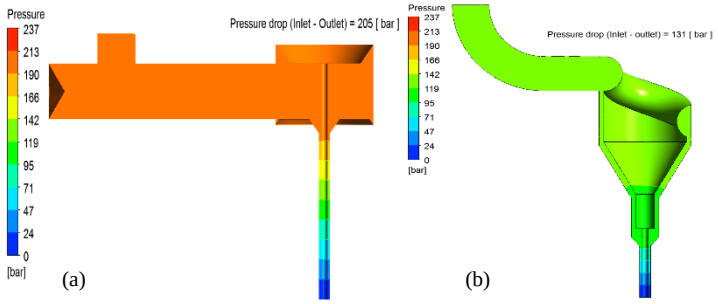

Figure 4: Pressure distribution for extrusion of the PLA at T = 200°C (U = 900 mm/min) (a) 1st generation CFC print head (b) modified side- fed CFC print head

The effect of the flow residence time is directly related to the velocity and local shear rate. Residence time becomes very large along the zone, where the velocity vanishes and has low wall shear rate. A very low residence time could indicate that some amount of the polymer may not have enough time to melt completely and high residence time implies the stagnation of the molten polymer in low local shear rate region. Since residence time distribution inside the geometry is one of the essential matters for quality of the extrudate, particle tracking simulations were conducted by using the mixing module and statistical functions of ANSYS Polystat. In order to investigate the residence time inside the geometry, 5000 particles were released from the inlet section and tracked until the nozzle exit.

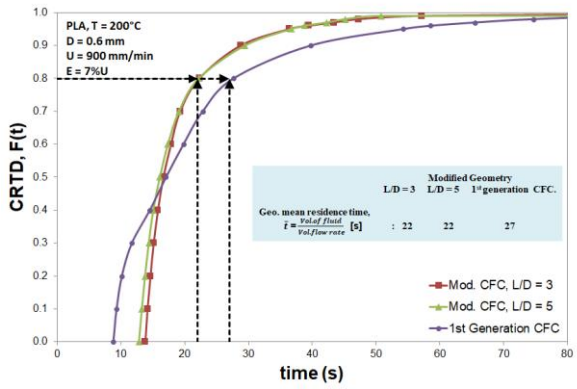

Figure 5: Cumulative residence time distribution function, F(t) of PLA at T = 200°C

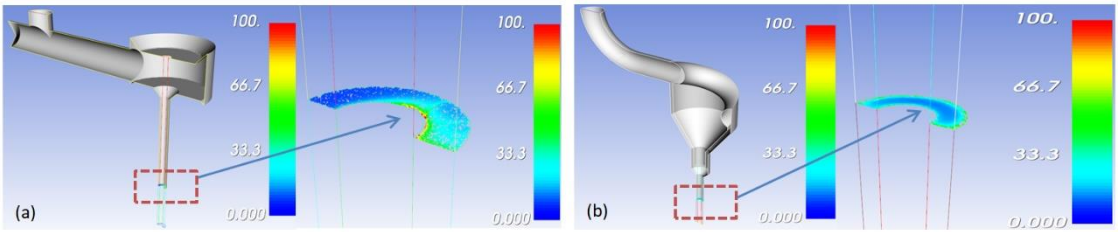

Figure 6: Particle tracking results of PLA at T = 200°C (fiber feed rate = 900 mm/min) (a) 1st generation CFC print head and (b) modified side- fed CFC print head with L/D = 5.

Figure 5, shows the result of the cumulative resident time distribution (CRTD) at the nozzle exit section for modified CFC print head and 1st generation print head. The majority of the particles exits the nozzle for both, modified CFC and 1st generation CFC print head, is relatively short, approximately 80% of the particles exit the nozzle in around 22 s and 27 s, which are analogous to the analytical calculation of geometrical mean residence time. Moreover, for a given feed rate, the average residence time is reduced by 18% for the modified CFC print head. Furthermore, in Figure 6 (a), 1st generation CFC print head, Non-uniform residence time distribution (highlighted) was detected in the exit section due to the unbalanced flow field. In addition, a small fraction of the particles in the core region (between CCF filament and plastic melt) have even longer residence time leading to uneven material coating of the extruded dual matrix composite. Furthermore, the particle tracking simulation infers that the optimization via modified print head yielded better and uniform residence time distribution along the nozzle, thus optimal utilization of the print head was achieved.

5.2 Pressure Drop and Extrudate Shape Prediction

In order to predict and determine the effect of viscoelasticity on the dual matrix extrusion process, besides the viscous model, the viscoelastic numerical simulations using multimode integral K-BKZ are considered. Furthermore, the current work comprising of all parametric studies concerning extrudate swell/shrinkage were performed using nozzles with the same diameter, 0.6 mm and various length to diameter (L/D = 3 and 5) ratios. Herein, by solving the model parametrically, a gradually increase in plastic- and fibers feed rates can be

achieved, and simultaneously investigate its influence on the quality of extruded dual matrix composite.

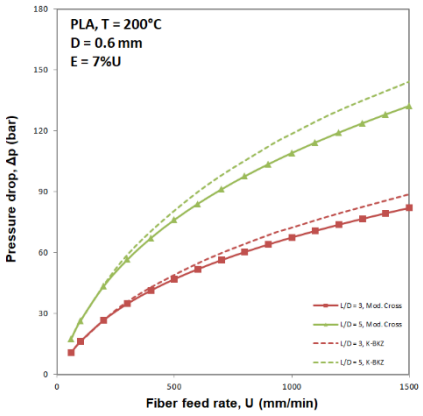

Figure 7: Predicted pressure drop as a function of the fiber feed rate along the nozzle using viscous- (solid symbol lines) and viscoelastic models (dashed lines) for PLA at T = 200°C

The pressure drops shown in Figure 7 were obtained from the resulting nozzle inlet and outlet melt pressure differential for the selected thermoplastic material. As expected, the use of long nozzle influenced in highest pressure drop in both viscous- and viscoelastic model, the predicted pressure drop from viscoelastic model tends to be higher than viscous model due to the extra- stress addition from the elastic part. Furthermore, pressure drop prediction using viscous- and viscoelastic models for the PLA matrix are identical up to fiber feed rate of 300 mm/min, with increase in feed rate difference between the two rheological models becomes significant. In order to have a consistent layer width during the printing and to avoid CCF filament buckling due to excess compression, the melt pressure should not exceed the critical value (Euler's buckling analysis) [7] and needs to be kept to a minimum. Hence the optimal feed rate for both, plastic and fiber, must be carefully selected so that excessive extrusion pressure can be avoided.

Since the print resolution is also affected by the ovality of the of dual matrix extrudate, predictions of extrudate swell based on different plastic feed rates were performed. Firstly, the results obtained by modified Cross model shown in Figure 8 (a) infers that the predicted plastic feed rate, E = 7 % configuration seems to be the optimized processing parameter in comparison to E = 6 %, shows a shrinkage behavior, whereas, E = 8 % shows more swell ratio.

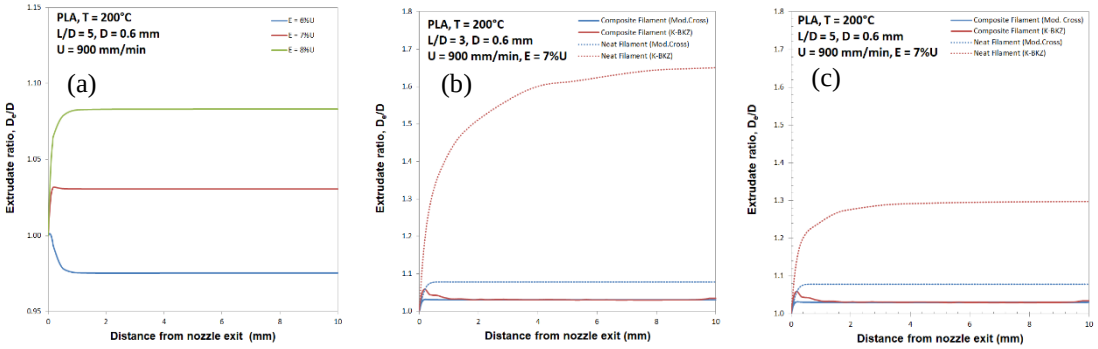

Figure 8: Predicted extrudate profiles, (a) viscous model for dual matrix composite, (b) viscous and viscoelastic models for dual matrix composite and neat filament with L/D = 3, (c) viscous and viscoelastic models for dual matrix composite and neat filament with L/D = 5

In order to check the effect of nozzle length on extrudate swell for composite and neat filament, simulations with and without the presence of reinforced fiber were conducted. Figure 8 (b) and Figure 8 (c) depicts the effect of rheology on extrudate profiles and their shape variation for two different L/D ratios. Furthermore, simulations show that the size of the extrudate was found to be larger right after exiting nozzle, due to the memory effects. Swelling behavior is well captured in viscoelastic model than the viscous model. Notably, in case of neat filament, the predicted extrudate swell by viscoelastic model is 53% (Nozzle L/D = 3) and 20% (Nozzle L/D = 5) higher than the value predicated by viscous model. Furthermore, with the longer nozzle land lengths, the memory effects declines, thus, promoting flow stability and reducing extrudate swell by 21%, especially for extruding neat filament. In case of composite filament, the extrudate swell predicted by viscoelastic model reaches its maximum value shortly after the nozzle exit, indicating that the memory effects fade away fast, and then flatten due to the drag of the reinforced fiber that restricts the mobility of the matrix. Generally, swell ratio decreases with increasing L/D ratio, but higher melt pressures and wall shear rate must be taken into consideration.

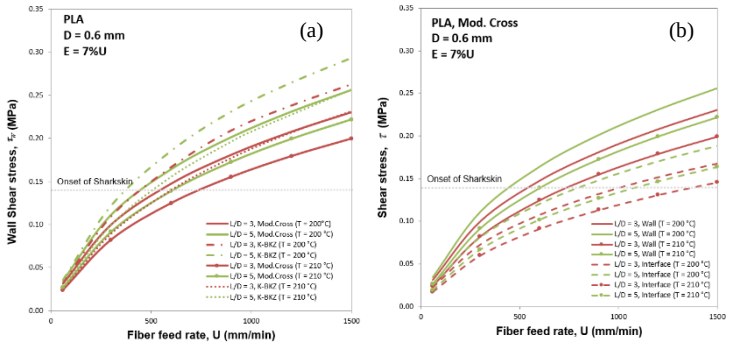

Figure 9: Predicted shear stress at two different temperatures for modified CFC print head with two different L/D ratios, a) predicted shear stress by viscous and viscoelastic model along the nozzle wall, (b) predicted shear stress by viscous model along the nozzle wall and melt-fiber interface

Since it is known that melt instability (surface roughness and melt fracture) can occur at high shear stress and it may hinder the optical and mechanical properties of the final extruded part.

Thus, a proper process parameter setting e.g. feed rate, temperature, are important aspects in limiting the resultant of the high shear stress.
Figure 9 (a) shows the predictions of shear stress for different L/D ratios by viscous and viscoelastic model along the nozzle wall at various fiber feed rates. As can be seen, the effect of rheology and processing condition are significant that extrusion instabilities during part printing could possibly occur, if the shear stress exceeds the critical value. One of the initial extrusion instabilities that may occur due to increasing feed rate is a "sharkskin effect", a phenomenon where the extrudate loss its surface gloss [8]. According to Kanev et al. and Vlachopoulos et al., the onset of sharkskin for most common polymers occurs at 0.14 to 0.18 MPa, beyond this value melt fracture is observed [9,10]. These critical values may be used as benchmark for regulating the print speed during printing. However, the increase in printing speed may aggravate the probability of occurrence of the extrudate distortion. Furthermore, the predicted shear stress by viscous model, for example, with L/D = 3 nozzle at 200 °C, feed rate up to 550 mm/min in modified CFC print head is a secure range, beyond which the probability of onset of sharkskin increases. However, if the process demands faster print rate then increasing temperature can be a quick solution in order to minimize shear stress as shown in Figure 9 (b), since the viscosity of molten polymer will become lower.

6 CONCLUSIONS

In the present work, the CFD simulation investigated with straight extrusion flow model with a heat transfer is an accurate characterization for CFC printing process which provides comprehensive data analytics and understanding related to design limitations. Analysis of the CFD simulation results revealed the design flaws in the 1st generation CFC print head, such as longer residence time, high pressure- drop, stagnated and recirculating melt regions. These bottlenecks were addressed in the newly designed, modified CFC print head where a side- fed mandrel is used to iron out the impeding issues, not only reduced the melt residence time, overall pressure drop but also helped in realizing the uniform melt distribution inside the melt chamber and the complete elimination of stagnation and recirculation of fully developed melt. The overall pressure- drop investigated in the modified CFC print head nozzles with different L/D ratios are in sync with the tolerance for the optimal print condition predicated on extrudate swell ratio and shear stress. The optimal printing setting for PLA in the modified CFC print head with nozzle of L/D = 5 is found to be in the range of 600 mm/min to 900 mm/min at 200 °C to 210 °C, respectively. In future, for the further references, the CFD modelling presented in the current research work may be considered as a benchmark for any given thermoplastic materials i.e., neat polymers or filled polymers.

7 ACKOWLEDGEMENT

The work for the project "3D-CFRP" was supported by the EU funded network M-Era.Net, the BMVIT (Austrian Ministry for Transport, Innovation and Technology), the FFG (Austrian Research Promotion Agency), as well as the RCL (Research Council of Lithuania) and FASIE (Foundation for Assistance to Small Innovative Enterprises, Russia).

REFERENCES

[1] R. Matsuzaki, M. Ueda, M. Namiki, T. K. Jeong, H. Asahara, K. Horiguchi, T. Nakamura, A. Todoroki, Y. Hirano, *Three-dimensional printing of continuous-fiber composites by in-nozzle impregnation*, Scientific Reports (2016)

[2] A. Bellini, S. Güçeri, M. Bertoldi, *Liquefier dynamics in fused deposition, Journal of Manufacturing Science and Engineering*, Transactions of the ASME (2004) 126:237-246

[3] B. N. Turner, R. Strong, S. A. Gold, *A review of melt extrusion additive manufacturing processes: I. Process design and modeling*, Rapid Prototyping Journal (2014) 20-3:192-204

[4] H. S. Ramanath, C. K. Chua, K. F. Leong, K. D. Shah, *Melt flow behaviour of poly-e-caprolactone in fused deposition modelling*, J Mater Sci: Mater Med (2008) 19:2541–2550

[5] H. M. Laun, *Prediction of Elastic Strains of Polymer Melts in Shear and Elongation*, Journal of Rheology (1986) 30: 459

[6] E. Mitsoulis, *50 Years of the K-BKZ Constitutive Relation for Polymers*, ISRN Polymer Science (2013): 22

[7] M. A. Yardimci, S. I. Guceri, *Numerical modeling of fused deposition processing*, Proceedings of the ASME Materials Division IMECE (1995) 69-2:1225-1235

[8] J. Molenaar, R. J. Koopmans, C. F. J. den Doelder, *Onset of the sharkskin phenomenon in polymer extrusion*, Physical Review E (1998) 58-4: 4683-4691

[9] D. Kanev, E. Takacs, and J. Vlachopoulos, *Rheological Evaluation and Observations of Extrusion Instabilities of Biodegradable Polyesters*, International Polymer Processing (2007) 22-5: 395-401

[10] J. Vlachopoulos, D. Strutt, *The Role of Rheology in Polymer Extrusion*. New Technology for Extrusion Conference. Italy, Milan (2003): 20-21